RSC Advances

PAPER

View Article Online
View Journal | View Issue

Cite this: *RSC Adv.*, 2021, **11**, 192

Excellent humidity sensor based on ultrathin HKUST-1 nanosheets†

Qiaoe Wang,[a] Meiling Lian,[b] Xiaowen Zhu[b] and Xu Chen *[b]

The copper-based MOF, HKUST-1 has been applied for humidity sensing owing to hydrophilic ligands and open metal sites which are suitable for sensitively detecting moisture. However, most of the research on the sensor HKUST-1 focuses on the role of the central metal. There are few reports on the morphology–activity relationship of HKUST-1. In this work, we synthesized two kinds of HKUST-1 including octahedral structures and ultrathin nanosheets, and systematically studied the performance of moisture sensing. Compared to HKUST-1 octahedra, HKUST-1 nanosheets showed lower and wider detectable humidity range, achieving a fast response. Starting from the exposed hydrophilic functional groups of HKUST-1 nanosheets, we have revealed that hydrophilic ligands play an important role in improving the adsorption capacity during the adsorption process. In addition, ultra-thin HKUST-1 nanosheets act as an excellent mass transfer medium, accelerating proton transfer and water molecule movement. To further improve the performance of the HKUST-1 humidity sensor, black phosphorus quantum dots (BPQDs) with a high surface reactivity were used to build a composite sensing platform. The excellent proton transfer capability of BPQDs leads to one order of magnitude improvement in the sensitivity of the BPQDs/HKUST-1 systems compared to HKUST-1 only.

Received 30th September 2020
Accepted 10th December 2020

DOI: 10.1039/d0ra08354b

rsc.li/rsc-advances

Introduction

Humidity detection is very important in agriculture and industrial fields, and weather monitoring. The development of new functional materials is a research hotspot of humidity sensors. A variety of materials have been used to build humidity sensors. A sensor based on an organic polymer conductive material has the advantage of high response magnification,[1,2] but its recovery and stability are poor, and the sensing material is susceptible to aging. Sensors based on nanomaterials such as graphene and MoS_2 can overcome the above disadvantages,[3,4] but their response time is not satisfactory. Although the improved WS_2 or black phosphorus flakes have faster response and recovery time,[5,6] the preparation is complicated and energy consumption is high, which limit the development and wide application of these materials. In recent years, there have been studies reporting new biomaterial-based sensors, but their high cost is also a problem that must be overcome.[7] Thus, developing low-energy-consuming and reliable humidity sensing materials is a requisite for humidity sensors.

Metal–organic frameworks (MOFs), which are a nanoporous crystalline materials, could effectively concentrate analyte molecules including volatile organic compounds, polyaromatic hydrocarbons, dyes, and moisture.[8] In addition, MOFs are also proton-conducting materials, which could be tuned by introducing hydrophilic units into their structure.[9] The hydrophilic oxygen atoms serve as hydrogen-bonding acceptors, meanwhile may also have contribution to introduce guests.[10] Although MOFs have been widely used in humidity sensors, they still have many problems, such as long response and recovery time, and low sensitivity.[11–13] In addition, the understanding of MOFs as moisture sensitive sensing elements is not profound enough.

HKUST-1, is a copper-based MOF with paddle-wheel-like coordination between Cu-dimers and four 1,3,5-benzenetricarboxylate (BTC) linkers.[14] It is advantageous that HKUST-1 has both oxygen-containing ligands and open metal sites, which render the adsorption of water molecules easier and more suitable for sensitive detection of moisture. Therefore, considering HKUST-1 as a model, we prepared ultrathin HKUST-1 nanosheets and octahedral bulk structures, and systematically studied their moisture sensing properties. Ultrathin HKUST-1 nanosheets are more sensitive to changes in humidity, and can detect a lower humidity with a wider linear range of sensing than octahedral bulk structures. For the excellent performance of the ultrathin HKUST-1 nanosheets, we also conducted in-depth exploration and reasonable explanation. In addition, in order to improve the performance of the humidity sensor based on HKUST-1, black phosphorus quantum dots (BPQDs)[15–18] with a high surface reactivity and

[a]Key Laboratory of Cosmetic, Beijing Technology and Business University, China National Light Industry, Beijing 100048, P. R. China

[b]State Key Laboratory of Chemical Resource Engineering, Beijing University of Chemical Technology, Beijing 100029, P. R. China. E-mail: chenxu@mail.buct.edu.cn

† Electronic supplementary information (ESI) available. See DOI: 10.1039/d0ra08354b

sensitivity to moisture were used as the sensibilization components to build a composite sensing platform.

Experimental

Reagents and materials

Red phosphorus was purchased from Aladdin (99.999% metal basis). Tin (Aldrich, powder, 99.99% trace metal basis) and iodine (Aldrich, 99.995% trace metal basis) were used as raw materials to produce black phosphorus. Polyvinylpyrrolidone (PVP, MW = 58 000), ascorbic acid, H_3BTC and other reagents were of analytical grade obtained from commercial suppliers and used as received. Deionized water was used in all the experiments.

Synthesis of black phosphorus (BP). The red phosphorus, tin and iodine used as the raw materials were weighed in a glove box, owing to their instability. The raw materials were carefully transferred to an ampule and the ampule was directly sealed before taking out of the glove box. Then, the sealed ampule was loaded in a muffle furnace for BP growth. The growth was carried out as described in a previous report.[19] Briefly, the temperature of the furnace was increased to 590 °C and maintained there for 2 h. Subsequently, the temperature was decreased to 485 °C and held for 2 h. Then, the temperature was decreased again to 120 °C. The ampule was retrieved and cooled naturally to room temperature. The BP microribbons were separated from the ampule by ultrasonicating with ethanol.

Synthesis of the black phosphorus quantum dots. The long BP microribbons were used to prepare well-dispersed BPQDs *via* solvothermal method.[20] Briefly, BP microribbons were ground into powders in *N*-methyl-2-pyrrolidone (NMP) for approximately 20 min. Then, the fine powders were transferred to a flask containing a saturated solution of sodium hydroxide in NMP. The suspension was stirred vigorously for 8 h at 150 °C in nitrogen atmosphere.

Synthesis of the ultrathin HKUST-1 nanosheets. In a modified synthesis of HKUST-1, the first step was to synthesize Cu_2O cubes.[21] Copper chloride dihydrate (0.1 mM) and polyvinyl pyrrolidone (0.1 g) were dissolved in deionized water (50.0 mL) and the resulting solution was stirred for 5 min. Then, 0.2 M NaOH was added dropwise at the rate of one drop per second. With continual stirring for 5 min, 2.5 mL of ascorbic acid (0.1 M) was added dropwise every three seconds. After stirring for another 5 min, the obtained product was rinsed twice with ethanol. The prepared Cu_2O ethanol suspension was used to synthesize HKUST-1 nanosheets. Polyvinyl pyrrolidone (0.4 g) was dissolved in 60.0 mL deionized water. Then, trimesic acid (H_3BTC, 0.2 g) was dissolved in 4 mL ethanol and mixed with the above solution. A white mixture formed was stirred for 5 min. An ethanol solution containing 10 mL of Cu_2O cubes was added to the above mixture, when the solution became clear in a min. After stirring for 14 h, the precipitate was rinsed thrice with ethanol.

Synthesis of the octahedral HKUST-1. $[Cu_3(BTC)_2(H_2O)_3]n$ crystals were prepared by a solvothermal reaction.[22] Briefly, $Cu(NO_3)_2 \cdot 3H_2O$ (4.5 mmol) was dissolved in 15 mL deionized water and H_3BTC (2.5 mmol) was dissolved in 15 mL ethanol. After stirring the mixture for 30 min, it was transferred to a Teflon autoclave liner and heated at 120 °C for 12 h. After cooling naturally to room temperature, blue powders were obtained. The powders were washed thrice with ethanol, and then dried overnight at 150 °C.

Humidity sensing measurements. The prepared composite and deionized water were mixed to form a paste. Then the paste was dip-coated on Ag–Pd interdigitated electrodes with ceramic as substrate (6 mm × 3 mm, 0.5 mm thick) to form a film. And then the film was dried in air at about 25 °C for 24 h. The humidity sensitive properties of the samples were investigated at 1.25 V AC under different relative humidity (RH) on the measuring system of Chemical Humidity Sensing-1 (CHS-1) at room temperature (25 °C) (Beijing Elite Tech. Co., Ltd., China). Various Relative Humidity (RH) levels from 11% to 95% RH were produced by diverse saturated salt solutions embracing LiCl for 11% RH, $MgCl_2$ for 33% RH, $Mg(NO_3)_2$ for 54% RH, NaCl for 75% RH, KCl for 85% RH, and KNO_3 for 95% RH. The saturated salt atmosphere was homogeneous and stable.

Apparatus

The Fourier transform infrared (FT-IR) spectra were measured on an FT-IR spectrometric spectrophotometer (Bruker VERTOR-22) (For FTIR, potassium bromide crystals are ground into powder and pressed into sheet. Then a certain amount of sample is dropped on the potassium bromide sheet, and the test is performed after it is completely dried). UV-vis spectra were measured by a spectrophotometer (UV-2501 PC, Shimadzu, Japan). Photoluminescence (PL) spectra were recorded on a spectrophotometer (RF-5301PC, Shimadzu, Japan). The morphology of the obtained nanomaterials was determined using a JEM-1011 electron microscope (TEM). Scanning electron microscopy (SEM) images were recorded on a Zeiss Supra 55 field emission scanning electron microscope using an accelerating voltage of 20 kV. The high-resolution transmission electron microscopic (HRTEM) images were performed on JEOL 2010 F. X-Ray powder diffraction (XRD) was carried out by a Rigaku diffractometer D/max-2500. The Raman spectra were recorded by a RENISHAW Via-Reflex Raman system. The humidity detection was carried out by CHS-1 Smart Humidity Analyzer. Contact angle measurement was operated on Surface Electro Optics, Model Phoenix-i system.

Results and discussion

Characterization of materials

The ultrathin HKUST-1 nanosheets were synthesized under mild conditions at room temperature (25 °C) whereas HKUST-1 octahedrons were prepared by solvothermal reaction. The synthesis of ultrathin HKUST-1 nanosheets is simple, however, the growth process is sensitive to temperature, stirring speed, and other parameters. As shown in Fig. 1a, under specific conditions, we successfully synthesized rectangular ultrathin HKUST-1 sheets. The synthetic approach to HKUST-1 blocks has matured, with the typical octahedral HKUST-1 shown in Fig. 1b. Fig. 1c and d show the simulated and experimentally recorded

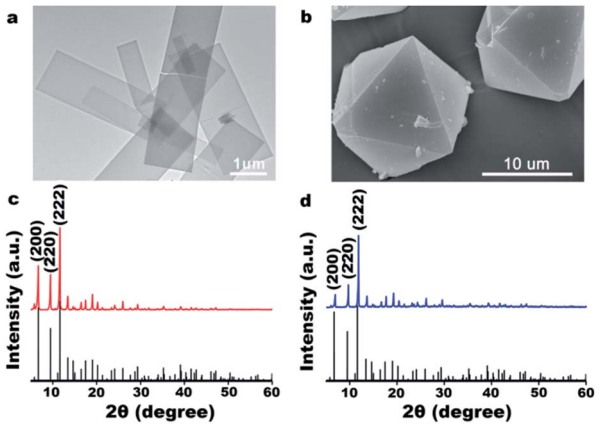

Fig. 1 TEM images (a and b) and XRD patterns (c and d) of the HKUST-1 nanosheets (a and c) and the HKUST-1 octahedron (b and d).

XRD patterns of the as-prepared ultrathin film and octahedral HKUST-1 sample. All the diffraction peaks of as-prepared ultrathin films and octahedral samples could be indexed to those of HKUST-1 and could also be matched well with the simulated patterns, showing the cubic crystal system and the $Fm\bar{3}m$ space group.[2]

Understanding the interaction between water molecules and humidity sensitive elements

HKUST-1 contains open metal sites to react with water vapor, whereas the carboxylic acid groups of the organic ligand render proton conduction possible. During a typical humidity sensing process, under a certain humidity environment, water molecules diffuse and adsorb on the active sites. Hydroxyl groups are formed after the water molecules dissociate into H^+ and OH^- under the high electrostatic fields; meanwhile, a monolayer is formed *via* chemisorption.[13] On the basis of chemical adsorption, the dissociated protons are transferred from the surface hydroxyls to adjacent water molecules to form hydronium ions (H_3O^+), and the physisorbed layers appear. The proton conduction could be achieved by releasing a proton from H_3O^+ to neighboring water molecules, meanwhile accept a proton from another donator (Fig. 2c).[13] The physisorbed layers thicken incessantly with an increase in the RH. Therefore, the ion conduction of the absorbed water molecules is enhanced, and consequently, the impedance values decrease significantly. The impedance plots of HKUST-1 reveals this process (Fig. 2a and b). When the RH is low, the conduction relies mainly on proton jump on the surface of HKUST-1; the corresponding curve is a straight line (Fig. S1†). The physical adsorption layers are stacked with increasing RH. More and more ionized water molecules make the impedance to continuously decline, which corresponds to the semicircular curve. At high RH, ionic conduction dominates the conduction mechanism, as indicated by a small tail appearing following the semicircle in the impedance plots. Unlike ultrathin HKUST-1 nanosheets, the impedance plots of octahedral HKUST-1 reveal that the conduction mechanism is mainly in the form of proton

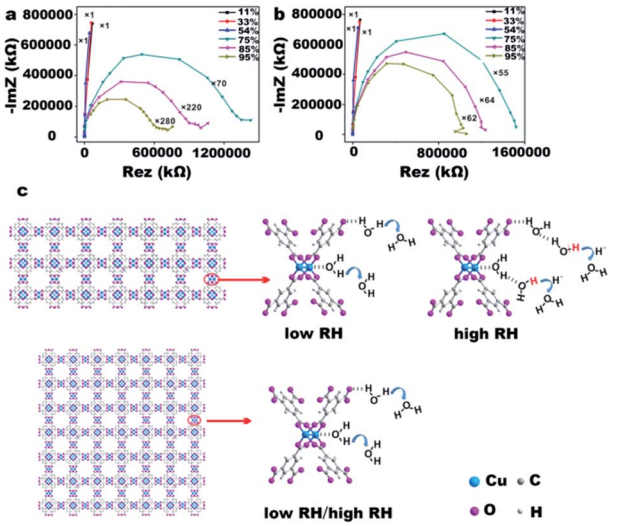

Fig. 2 The impedance plots of HKUST-1 nanosheets (a) and HKUST-1 octahedron (b), (c) Schematic illustration of conduction process for HKUST-1 nanosheets and octahedral HKUST-1. The enlarged view for the 11, 33 and 54% RH in (a) and (b) are listed in Fig. S1.†

conduction (Fig. 2b). Compared to octahedral HKUST-1, the conductivity of ultrathin HKUST-1 nanosheets is significantly better (Fig. 2a). A large number of adsorbed water molecules are ionized at RH 75% and the conduction mechanism gradually shifts from proton conductivity to ionic conductivity.

However, according to our observations, different morphologies of the same type of MOFs do not only have difference conduction mechanisms but also exhibit significant differences in the sensitivity, response and recovery time, and detectable humidity range during the humidity cycle (Fig. 3a and b). Fig. 3a

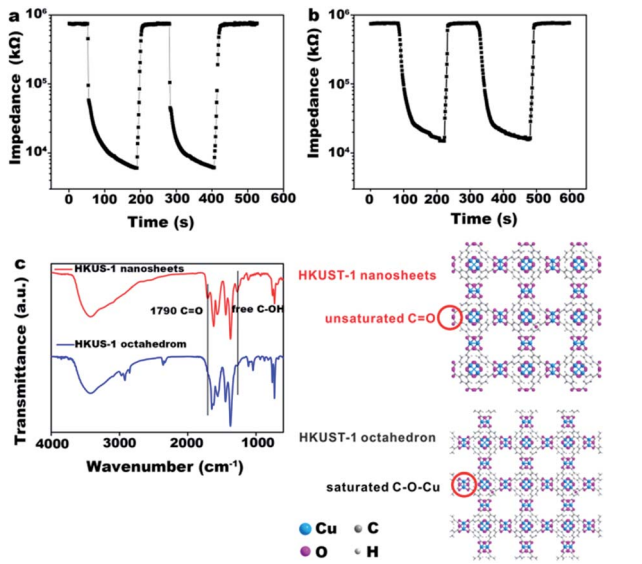

Fig. 3 The response and recovery characteristics of HKUST-1 nanosheets (a) and HKUST-1 octahedron (b), (c) the FT-IR spectra of HKUST-1 nanosheets and HKUST-1 octahedron. The different bonding states for functional groups of HKUST-1 nanosheets and HKUST-1 octahedron reflected by FT-IR spectrum are showed in diagram.

shows the response and recovery characteristics of sensors based on ultrathin HKUST-1 nanosheets when the RH changes from 11 to 95%. The sensitivity of ultrathin HKUST-1 nanosheets is 1×10^2. Ultrafast response time (2 s) and recovery time (15 s) could be obtained, while the relative humidity was increased from 11 to 95% and then back to 11%. The excellent mass transfer capability of the ultrathin HKUST-1 nanosheets leads to improvement in the sensitivity of the HKUST-1 nanosheets by an order of magnitude than that of octahedral HKUST-1 (1×10^1) (Fig. 3b). Octahedral HKUST-1 shows a longer response time of 18 s, however, surprisingly, the recovery time (11 s) is faster than that of the ultrathin HKUST-1 nanosheets (15 s). Disregarding the interferences of different metal centers and ligands, the most plausible reasons for the differences in the moisture sensitivity could be attributed to the different macrostructures of the two HKUST-1 samples which directly affect the interaction with the water molecules. Therefore, it is necessary to analyze the structural characteristics of the two HKUST-1 samples and their interaction with water molecules.

In a vapor-filled atmosphere, water molecules first diffuse into the material. We speculate that the diffusion of water molecules toward the ultrathin two-dimensional plane would be more facile than into a three-dimensional bulk material. Along the pathway the water molecule passes through, a single chemical adsorption layer forms and then physical adsorption occurs. One could speculate that, in case of the ultrathin HKUST-1 nanosheets, this series of chain reactions occurs faster than in octahedral HKUST-1. The rapid response can be attributed to the dominant physical adsorption of water and the thinness of the film. Surprisingly, careful observations indicate that the recovery time for ultrathin HKUST-1 nanosheets is longer than that for the octahedral HKUST-1, which is in conflict with the previous discussion. We hypothesized that various morphologies may affect the internal chemistry differently, resulting in differences in the macro performance.

MOFs with open metal sites are very beneficial for the direct interaction between metal centers and adsorbates. The coordinately unsaturated copper sites of HKUST-1 are the preferential adsorption sites that are occupied by adsorbed water.[23] The adsorbed water molecules would coordinate with the open metal sites, following which the central Cu^{2+} ions would acidify the coordinated water molecules to contribute protons.[24] The coordination of water molecules as proton donors could improve the proton conductivity.[24] However, the copper sites are approachable from the main pores only, but not from the pores enclosed by the benzene ring.[23] Moreover, for the same paddle wheel unit formed by copper formate of HKUST-1, the adsorption of the second water molecule is weaker than that of the first one.[25] That is, although the open Cu^{2+} center is a preferential adsorption site, the adsorbed water molecules also contribute to proton conduction. The adsorption capacity of Cu^{2+} for water molecules is limited.

An experimental and theoretical study on the adsorption of CO_2 based on CuBTC was presented by Nachtigall *et al.*[26] For CO_2, CuBTC has three adsorption sites. At a lower coverage, CO_2 molecules adsorb preferentially on the coordinatively unsaturated metal sites. However, at higher coverages, CO_2 molecules enter into the tetrahedral cage and adsorb on "cage window sites" and "cage center sites". Taking CO_2 as a reference, HKUST-1 may also have heterogeneous adsorption sites for water vapor molecules in case of increased coverage. The adsorption properties of HKUST-1 are not due to open Cu^{2+} sites only, van der Waals interactions and hydrogen bonds also contribute to the adsorption at high coverages.[27]

H_3BTC as ligand has hydrophobic phenyl rings suppressing the cohesion of adsorbed water vapor molecules whereas the hydrophilic oxygen atoms of carboxyl groups offer van der Waals forces and hydrogen bonds which render HKUST-1 conducive to both adsorption and desorption of water molecules.[8] At moderate and high humidity, the possible hydrogen bonding network would facilitate direct interaction between the moisture-sensitive material and water molecules. Moreover, the free carboxylic acids potentially act as proton carriers and active sites.[10]

In the previous discussion, we analyzed the affinity of the ligand trimellitic acid for water adsorption. Hydrophilic oxygen atoms of carboxyl groups have the potential to combine with water molecules by van der Waals forces and forming hydrogen bonding. Since the nanosheets have an extended planar structure, more functional groups may be exposed, whereas these active sites are buried within the octahedral bulk structures. This speculation was confirmed by FT-IR of ultrathin HKUST-1 nanosheets and octahedral HKUST-1 (Fig. 3c). The asymmetric stretching at 1500–1600 cm^{-1} is attributed to the carboxylate groups and the corresponding symmetric stretching of the carboxylate groups occurs at 1314–1470 cm^{-1}.[8] Since HKUST-1 contains open metal sites to coordinate with water molecules, the bending mode of molecular water is observed at 1620 cm^{-1}.[28] The bands at 1710 and 1280 cm^{-1} are assigned to the stretching vibration frequencies of free C=O and C–OH groups, respectively.[29,30] It is noteworthy that these two characteristic peaks could be clearly observed in the FT-IR spectrum of the ultrathin HKUST-1 nanosheets, whereas could not be found in the FT-IR spectrum of the octahedral HKUST-1. In other words, the two-dimensional HKUST-1 nanosheets exposed more uncoordinated active groups of ligands than the tightly packed three-dimensional bulk material. These groups, serving as active sites, essentially contribute to the formation of hydrogen bonds with water molecules and act as proton carriers.

Owing to the ultrathin and two-dimensional planar structure, HKUST-1 nanosheets expose more active sites, resulting in better hygroscopic properties than those of the octahedral HKUST-1 and exactly manifest the principle of "structure dictates function".[21] Stronger interactions between the ultrathin HKUST-1 nanosheets and guest molecules induce the ultrathin HKUST-1 nanosheets to have a longer desorption process. According to this idea, we can also explain the rapid response characteristic of ultrathin HKUST-1 nanosheets. At the best test frequency (Fig. S2,† ultrathin HKUST-1 nanosheets exhibit a higher sensitivity, lower detectable relative humidity, and wider humidity detection range than those of octahedral HKUST-1 (Fig. S3 and S4†).

Introducing BPQDs for sensibilization

Through extensive research on the synthesis of black phosphorus, we adopted a simple method to produce multilayered bulk black phosphorus.[19] The crystalline structure of the as-grown black phosphorus long microribbons was revealed by XRD (Fig. S5a†). Only the characteristic (020), (040), and (060) diffraction peaks of black phosphorus could be observed, implying that no impurities such as tin, iodine, tin–iodide, or tinphosphide remained.[19] Fig. S5b† shows the Raman spectra of bulk BP bulk (red line) and BPQDs (blue line). Three prominent peaks of bulk BP bulk and BPQDs can be ascribed to one out-of-plane phonon modes (A_g^1) and two in plane modes, that is, B_{2g} and A_g^2.[31] Compared to the bulk BP (A_g^1 at 356.2, B_{2g} at 435.2, and A_g^2 at 463.7 cm^{-1}), the three modes of the BPQDs are red-shifted by around 5.6, 3.8, and 3.3 cm^{-1}, respectively. This is probably due to the thin thickness and small lateral dimensions of the QDs. The hierarchical structure of BP can be clearly observed in the SEM image (Fig. S5c†). Compared to the quantum dots, bulk black phosphorus has the disadvantage of high price and low yield. Meanwhile, the one-step synthesis of BPQDs provides a high yield as well as a larger specific surface area and higher reactivity than bulk BP. The synthesized BPQDs are monodisperse nanoparticles with a near-spherical morphology and a diameter of 3.5–5.5 nm (Fig. 4a and S6†). The UV-vis absorbance spectrum of BPQDs shows a broad absorbance ranging from 200 to 700 nm, indicating potential application in photothermal therapy (Fig. 4b). The fluorescence emission spectra of BPQDs were recorded with 400, 410, 420, 430, 440, 450, 460, and 470 nm excitation wavelengths (Fig. 4b). The emission peak positions do not significantly shift upon changing the excitation wavelength. BPQDs have a discernible lattice structure and the lattice fringes of 0.25 nm attributed to the (111) planes of the BP could be observed (Fig. 4a).[18] The ultra-small and well-crystallized quantum dots could be potentially applied in the sensing field.

The abundant surface lone pair electrons of BPQDs render them very sensitive to moisture. The sensors based on BPQD can obtain ultra-fast response time (2 s) and recovery time (4 s), and the humidity hysteresis is almost negligible, which shows that BPQD is an excellent humidity-sensitive material (Fig. S7a†).The impedance spectra of BPQDs shows that the conduction mechanisms include proton conduction and ion conduction at different RH similar to that observed for HKUST-1 nanosheets (Fig. S7b and c†). Herein, we predict that the sensitive BPQDs could be used to optimize the performance of the humidity sensor of HKUST-1. As predicted, the excellent proton transfer capability of BPQDs leads to an improvement in the sensitivity of the BPQDs/HKUST-1 nanosheets and BPQDs/HKUST-1 octahedron systems by an order of magnitude (1×10^3 and 1×10^2, respectively) compared to HKUST-1 only (Table S1†). For BPQDs/HKUST-1 nanosheets, quick response and recovery time (3 and 7 s, respectively) are achieved. BPQDs/octahedral HKUST-1 show a longer response time (15 s) and recovery time (24 s). After introducing BPQDs, the impedance spectra and humidity hysteresis show no significant changes (Fig. S8–S10†).

Additionally, the surface of BPQDs can be oxidized when exposed to water molecules. However, phosphorus oxides would promote the adsorption of water molecules. Besides, hydrogen bonds could be formed to enhance the interaction with water molecules. The BPQDs have issues related to environmental instability, which is well-known. In this study, we also considered the reliability of the BPQDs/HKUST-1 nanosheets humidity sensor. NMP, which is used as a common stripping solvent for 2D materials, plays the role of a stabilizing solvent as well. Fig. S11† shows the UV-vis absorption spectrum of a fresh batch of BPQDs exposed to the air and light for 24 h and then stored in NMP or ethanol. After exposure to the air and light for 24 h, UV-vis absorption intensity slightly decreased for BPQDs stored in NMP whereas a significant decrease is observed for BPQDs stored in ethyl alcohol. In addition, porous HKUST-1 nanosheets have a strong affinity for NMP and can instantly absorb NMP (Fig. S12†). At this point, NMP acts as a carrier to transport BPQDs into the HKUST-1 nanosheet layers and aids the BPQDs to bind tightly to MOFs. When BPQDs are below the layers of HKUST-1 nanosheets, owing to the lack of infiltration and adhesion, the moisture sensitivity is not as good as HKUST-1 nanosheets as bottom layers (Fig. S12†).

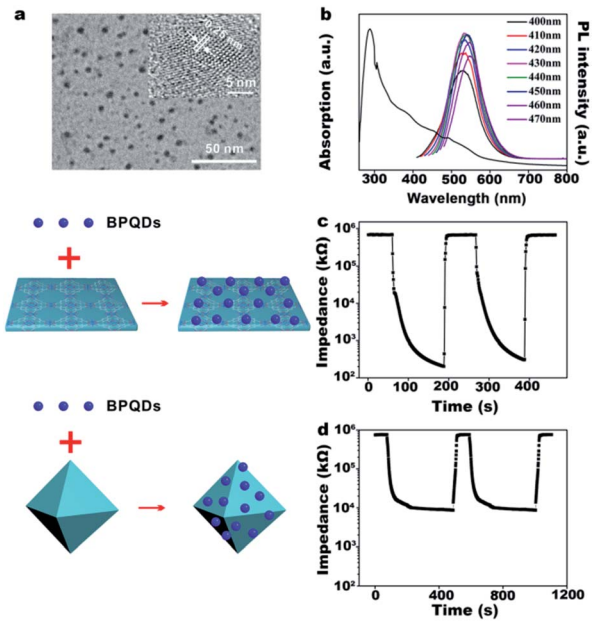

Fig. 4 (a) TEM image of the BPQDs. Inset: the lattice fringes of BPQDs. (b) PL emission spectrum and UV-vis absorption of BPQDs. The response and recovery characteristics of BPQDs/HKUST-1 nanosheets (c) and BPQDs/HKUST-1 octahedron (d).

Conclusions

Ultrathin HKUST-1 nanosheets with unsaturated metal sites and carboxyl groups of the ligands with hydrophilic oxygen atoms have been applied to humidity sensing. Owing to the ultrathin and plane structure, more active sites could be exposed than those exposed in octahedral bulk structures, as confirmed by FT-IR spectroscopy. These active sites facilitate the interaction of ultrathin HKUST-1 nanosheets with water

molecules. Therefore, the ultrathin HKUST-1 nanosheets show a longer desorption process as well as a rapid response owing to stronger adsorption of water molecules. Moreover, ultrathin HKUST-1 nanosheets serve as an excellent mass transfer medium, accelerating proton transfer and water molecule movements. For HKUST-1 nanosheets, as the relative humidity increases, the conduction mechanism changes from proton conduction to ion conduction whereas the conduction mechanism of octahedral HKUST-1 mainly relies on proton conduction. Therefore, HKUST-1 nanosheets could detect a lower humidity with a wider linear range of sensing compared to octahedral bulk structures. To improve the performance of the HKUST-1 humidity sensor, BPQDs with a high surface reactivity and sensitivity to moisture were used to build a composite sensing platform. The moisture-sensitive BPQDs improve the sensitivity of the BPQDs/HKUST-1 nanosheets and BPQDs/HKUST-1 octahedron by an order of magnitude. Given that BPQDs are very sensitive to air and water, their degradation would occur after prolonged exposure to air. Use of NMP as a protective agent and the surface oxidation of BPQDs were considered. Slight surface oxidation could enhance the affinity of BPQDs for water molecules without significant degradation.

Conflicts of interest

There are no conflicts to declare.

Acknowledgements

This work was supported by the National Natural Science Foundation of China (21874005) and the Open Research Fund Program of Key Laboratory of Cosmetic (Beijing Technology and Business University), China National Light Industry (No. KLC-2019-ZD3).

References

1 B. Chethan, H. G. Raj Prakash, Y. T. Ravikiran, S. C. Vijaya Kumari, S. Manjunatha and S. Thomas, *Talanta*, 2020, **215**, 120906.
2 H. S. Jung, P. Verwilst and W. Y. Kim, *Chem. Soc. Rev.*, 2016, **45**, 1242.
3 M. Cho, S. Kim, I. Kim, E. Kim and J. Oh, *Adv. Funct. Mater.*, 2020, **30**, 2070017.
4 J. Zhao, N. Li, H. Yu, Z. Wei, M. Liao and P. Chen, *Adv. Mater.*, 2017, **29**, 1702076.
5 H. Guo, C. Lan and Z. Zhou, *Nanoscale*, 2017, **9**, 6246.
6 D. Yu, J. Li, T. Wang, X. She and D. Yang, *Phys. Status Solidi RRL*, 2020, 1900697.
7 N. A. Carter and T. Z. Grove, *J. Am. Chem. Soc.*, 2018, **140**, 7144.
8 N. Hanikel, S. P. Mathieu and O. M. Yaghi, *Nat. Nanotechnol.*, 2020, **15**, 1.
9 P. Ramaswamy, N. E. Wong and B. S. Gelfand, *J. Am. Chem. Soc.*, 2015, **137**, 7640.
10 M. Sadakiyo, H. Ōkawa and A. Shigematsu, *J. Am. Chem. Soc.*, 2012, **134**, 5472.
11 A. Weiss, N. Reimer and N. Stock, *Micropor. Mesopor. Mat.*, 2016, **220**, 39.
12 A. A. Miguel, T. V. Mani, S. G. Surya, O. Shekhah, K. N. Salama, C. Serre, M. Eddaoudi, O. Roubeau and I. Gascón, *ACS Appl. Mater. Inter.*, 2020, **12**, 4155.
13 S. Rauf, M. T. Vijjapu, M. A. Andrés, I. Gascón, O. Roubeau, M. Eddaoudi and K. N. Salama, *ACS Appl. Mater. Inter.*, 2020, **12**, 29999.
14 H. K. Kim, W. S. Yun and M. B. Kim, *J. Am. Chem. Soc.*, 2015, **137**, 10009.
15 M. Pumera, *TrAC Trends Anal. Chem.*, 2017, **93**, 1.
16 A. Castellanos-Gomez, *J. Phys. Chem. Lett.*, 2015, **6**, 4280.
17 J. Miao, L. Cai, S. Zhang, J. Nah, J. Yeom and C. Wang, *ACS Appl. Mater. Inter.*, 2017, **9**, 10019.
18 C. Zhu, F. Xu, L. Zhan, M. Li, J. Chen, S. Xu, G. Huang, W. Chen and L. Sun, *Chem. -Eur. J.*, 2016, **22**, 7357.
19 M. Zhao, H. Qian, X. Niu, W. Wang, L. Guan, J. Sha and Y. Wang, *Cryst. Growth Des.*, 2016, **16**, 1096.
20 Y. Xu, Z. Wang, Z. Guo, H. Huang, Q. Xiao, H. Zhang and X. F. Yu, *Adv. Optical. Mater.*, 2016, **4**, 1223.
21 G. Zhan and H. C. Zeng, *Adv. Funct. Mater.*, 2016, **26**, 3268.
22 F. Ke, L. G. Qiu, Y. P. Yuan, F. M. Peng, X. Jiang, A. J. Xie, Y. H. Shen and J. F. Zhu, *J. Hazard. Mater.*, 2011, **196**, 36.
23 N. C. Burtch, H. Jasuja and K. S. Walton, *Chem. Rev.*, 2014, **114**, 10575.
24 N. C. Jeong, B. Samanta, C. Y. Lee, O. K. Farha and J. T. Hupp, *J. Am. Chem. Soc.*, 2011, **134**, 51.
25 L. Grajciar, O. Bludsky and P. Nachtigall, *J. Phys. Chem. Lett.*, 2010, **1**, 3354.
26 L. Grajciar, A. D. Wiersum, P. L. Llewellyn, J. S. Chang and P. Nachtigall, *J. Phys. Chem. C*, 2011, **115**, 17925.
27 S. Bordiga, L. Regli, F. Bonino, E. Groppo, C. Lamberti, B. Xiao, P. S. Wheatley, R. E. Morris and A. Zecchina, *Phys. Chem. Chem. Phys.*, 2007, **9**, 2676.
28 J. B. DeCoste, G. W. Peterson, B. J. Schindler, K. L. Killops, M. A. Browe and J. J. Mahle, *J. Mater. Chem. A*, 2013, **1**, 11922.
29 F. Wang, H. Guo, Y. Chai, Y. Li and C. Liu, *Micropor. Mesopor. Mat.*, 2013, **173**, 181.
30 Y. Liu, T. Zhang, W. Wu, S. Jiang, H. Zhang and B. Li, *RSC Adv.*, 2015, 56020.
31 Z. Zhang, X. Xin, Q. Yan, Q. Li, Y. Yang and T. L. Ren, *Sci. China Mater.*, 2016, **59**, 122.